HHS Public Access

Author manuscript

Nat Biomed Eng. Author manuscript; available in PMC 2021 March 28.

Published in final edited form as:

Nat Biomed Eng. 2021 January ; 5(1): 26–40. doi:10.1038/s41551-020-00621-9.

A microfluidic cell-migration assay for the prediction of progression-free survival and recurrence time of patients with glioblastoma

Bin Sheng Wong[1,2,&], **Sagar R. Shah**[3,4,&], **Christopher L. Yankaskas**[1,2,&], **Vivek K. Bajpai**[5,6], **Pei-Hsun Wu**[1,2], **Deborah Chin**[1], **Brent Ifemembi**[1,2], **Karim ReFaey**[4], **Paula Schiapparelli**[4], **Xiaobin Zheng**[7], **Stuart S. Martin**[8], **Chen-Ming Fan**[7], **Alfredo Quiñones-Hinojosa**[4,*], **Konstantinos Konstantopoulos**[1,2,3,9,*]

[1]Department of Chemical and Biomolecular Engineering, The Johns Hopkins University, Baltimore, MD 21218, USA.

[2]Institute for NanoBioTechnology, The Johns Hopkins University, Baltimore, MD 21218, USA.

[3]Department of Biomedical Engineering, The Johns Hopkins University School of Medicine, Baltimore, MD 21218, USA.

[4]Department of Neurosurgery, Mayo Clinic, Jacksonville, FL 32224, USA

[5]Department of Chemical and Systems Biology, Stanford University, Stanford, CA 94305, USA

[6]Institute for Stem Cell Biology and Regenerative Medicine, Stanford University School of Medicine, Stanford, CA 94305, USA

[7]Department of Embryology, Carnegie Institution for Science, Baltimore, MD 21218, USA

[8]Marlene and Stewart Greenebaum National Cancer Institute Comprehensive Cancer Center, Department of Physiology, University of Maryland School of Medicine, Baltimore, MD 21201, USA.

[9]Department of Oncology, The Johns Hopkins University, Baltimore MD 21205, USA

[*]Corresponding authors, konstant@jhu.edu (K.K.); Quinones-Hinojosa.Alfredo@mayo.edu (A.Q.H).

Author contributions

B.S.W., S.R.S., A.Q.H. and K.K. designed the study. B.S.W. performed most experiments, interpreted the data and wrote the manuscript. S.R.S. performed select experiments, conducted patient clinical analysis and assisted in writing the manuscript. C.L.Y. performed experiments using MAqCI, the transwell assay and isolation of cells for RNAseq and contributed to data analysis. D.C. performed select experiments. P-S.W. and B.I. performed survival analysis based on RNAseq data. K.R. and P.S. contributed to the design of the study and collected patient data. S.S.M. designed and provided support for the transwell-migration assay, while V.K.B., C.F. and X.Z. performed the RNA-seq experiments and analysis. All authors interpreted data, provided critical insights, and edited the manuscript. K.K. supervised the study, and wrote the manuscript.

[&]These authors contributed equally

Competing interests

MAqCI is the subject of US Utility Patent applications 15/780,768 and 14/906,055.

Additional information

Supplementary information is available for this paper at https://doi.org/10.1038/s41551-01X-XXXX-X.

Reprints and permissions information is available at www.nature.com/reprints.

Publisher's note: Springer Nature remains neutral with regard to jurisdictional claims in published maps and institutional affiliations.

Abstract

Clinical scores, molecular markers and cellular phenotypes have been used to predict clinical outcomes of patients with glioblastoma. However, their clinical use has been hampered by confounders such as patient co-morbidities, by the tumoral heterogeneity of molecular and cellular markers, and by the complexity and cost of high-throughput single-cell analysis. Here, we show that a microfluidic assay for the quantification of cell migration and proliferation can categorize patients with glioblastoma according to progression-free survival. We quantified with a composite score the ability of primary glioblastoma cells to proliferate (via the protein biomarker Ki-67) and to squeeze through microfluidic channels, mimicking aspects of the tight perivascular conduits and white-matter tracts in brain parenchyma. The assay retrospectively categorized 28 patients according to progression-free survival (short-term or long-term) with an accuracy of 86%, predicted time to recurrence, and prospectively categorized five additional patients on the basis of survival. RNA sequencing of the highly motile cells revealed differentially expressed genes that correlated with poor prognosis. Our findings suggest that cell-migration and proliferation levels can predict patient-specific clinical outcomes.

Glioblastoma (GBM) is the most common and aggressive type of primary brain cancer in adults, accounting for about 15–20% of all brain malignancies[1]. Owing to its highly proliferative and infiltrative nature, the median survival of GBM patients is only approximately 14.6 months, with less than 5% of patients surviving past 5 years[1,2]. GBMs invade locally into the surrounding brain parenchyma and frequently spread to the contralateral hemisphere through the corpus callosum, thereby confounding local therapy and rendering gross total resection nearly impossible[2–4]. As a result, despite aggressive radical surgical resection coupled with concurrent chemo- and radio- therapy, GBMs remain incurable and recur frequently[5].

To date, there is a lack of testing technologies that can effectively predict GBM outcomes in a patient-specific manner. While certain demographic (e.g. age), tumour (e.g. tumour locations, cytologic and histologic compositions) and clinical parameters (e.g. Karnofsky Performance Score) have demonstrated some prognostic values for survival correlation, they are often confounded by patient comorbidities, and thus rarely affect GBM treatment decision[5,6]. Recent advancements in proteomics and genomics have identified certain molecular markers, such as O^6-methylguanine DNA-methyltransferase (MGMT) promoter methylation and isocitrate dehydrogenase 1 (IDH1) mutation status, as independent prognostic factors for gliomas[7–14]. MGMT promoter methylation has been shown to be associated with longer overall survival and enhanced sensitivity to therapy[15–18]. However, inter- and intra- tumoral heterogeneity coupled with the lack of standardization and reproducibility of MGMT methylation status classification have prevented its widespread use in the clinic[19,20]. IDH1 mutation status has emerged as a leading prognostic marker for gliomas. Specifically, low-grade glioma patients harbouring the mutant form of IDH1 have improved prognosis and median survival compared to those expressing the wildtype IDH1[21]. Yet, the prognostic power of IDH1 mutation status on primary GBMs remains limited as IDH1 mutations are often associated with lower grades diffuse gliomas (Grade II and III) and with secondary GBMs[22–24]. Finally, the use of laborious and time-consuming *ex vivo*

expansion of cancer cells in murine xenograft model for phenotypic testing is impractical for informing patient care given the short survival span of GBM patients[25].

Cell population-based molecular analysis techniques often overlook the inherent diversity of cancer cells and suffer from the inability to discern inter- and intra- tumoral heterogeneity that may contribute to the aggressiveness of GBMs[26]. While high-throughput single-cell genomic and proteomic analyses could potentially ameliorate the problem of tumour heterogeneity, these techniques require sophisticated and expensive equipment and facilities, rendering their widespread application currently infeasible in most clinical settings[27,28]. Importantly, the aggressiveness of cancers is frequently a result of an amalgamation of multiple distinct combinations of genetic and proteomic alterations, which cannot be predicted accurately by just one or two molecular markers and might be difficult to decipher[29]. The heterogeneous and complex nature of GBMs therefore necessitates the development of a more direct, faster, inexpensive, high-throughput and unbiased *in vitro* testing technology for GBM prognosis capable of dissecting the heterogeneity among the cancer cells derived from individual patients. It is known that highly metastatic subpopulations of cancer cells have enhanced motility and proliferation rates that are linked to the aggressiveness and invasiveness of the cancer[30,31]. Along these lines, we have successfully developed a Microfluidic Assay for Quantification of Cell Invasion (MAqCI) to measure both the migratory and proliferative potentials of breast cancer cells for the purpose of assessing their metastatic propensity and screening of potential antimetastatic therapeutics[32]. We therefore hypothesized that MAqCI could be leveraged to identify a subpopulation of migratory and proliferative cells within a GBM patient-derived specimen whose prevalence would serve as a metric for predicting the aggressiveness of the disease and clinical prognosis.

Herein, we utilized the MAqCI technology to concurrently evaluate the migratory and proliferative potentials of patient-derived primary GBM specimens. MAqCI consists of two parallel seeding and media channels connected by a series of 10 μm-high Y-shaped microchannels with 20 μm-wide feeder channels bifurcating into 10 μm- and 3 μm-wide branches (Fig. 1A)[32,33]. These microchannels aim to recapitulate aspects of the complex topography and confining longitudinal pores or perivascular tracks of the brain parenchyma formed between glial cells and the basement membrane of vascular smooth muscle cells which ranges from 10–300 μm^2 in cross-sectional area[34]. By quantifying the relative abundance of highly motile cells that have successfully traversed the Y-shape microchannels as well as the proliferative potential of this migratory subpopulation, we demonstrate that MAqCI predicted individual patient survival and time to recurrence with high sensitivity, specificity and accuracy in a retrospective patient cohort. Furthermore, in a pilot prospective study, MAqCI classified all patients accurately based on their survival outcomes. RNA sequencing of isolated highly motile was compared to unsorted bulk GBM cells and revealed a group of differentially expressed genes (DEGs) whose individual expression patterns matched those of GBM patients with reduced overall survival. In sum, our study suggests that invasive spread and tumour growth are primary hallmarks of tumour aggressiveness, which can be exploited to accurately predict patient clinical outcomes.

Results

Quantification of GBM cell migration and proliferation.

To assess the capacity of MAqCI to predict individual GBM patient outcomes, we evaluated the migratory and proliferative potentials of patient-derived primary GBM cells. All cells that enter the feeder channels were analysed and classified into 2 categories based on their migratory behaviours: lowly motile cells are defined as cells that migrated into the feeder channels but failed to reach and/or enter the bifurcations, while highly motile cells are defined as cells that successfully traversed the entire length of the feeder channels and entered either one of the branch channels (Fig. 1A, Supplementary Video 1). Using live-cell imaging, we calculated the percentage of highly motile cells that migrated in the microchannels, and the percentage of these highly motile cells that preferentially entered the narrower 3 μm-wide branches (termed as percentage of narrow entry). Laminin was used to coat MAqCI as it is an extracellular matrix protein that is enriched in the white matter tracts and vascular basement membrane of the brain parenchyma[35] and promoted the most efficient migration in our patient-derived primary GBM cells over other substrates, such as collagen and fibronectin (Supplementary Fig. 1A). The widths of the microchannels in MAqCI ranged from 3 to 20 μm to recapitulate the relevant dimensions of diverse *in vivo* pre-existing tissue tracks as measured by intravital microscopy[36]. The 3 μm channels were created specifically to evaluate the ability for GBM cells to deform their cytoskeleton and nucleus to enter into tight constrictions. We hypothesize that the ability of cells to deform and migrate in confining microenvironments could correlate with their aggressiveness and invasiveness. Interestingly, we observed the same values of percentage of highly motile cells in symmetrical 10/10 μm branch channels and the 3/10 μm asymmetrical design (Supplementary Fig. 1B). This result suggested that a symmetrical branch provides identical information as the asymmetrical design in terms of the percentage of highly motile cells, but less information in terms of the cell's ability to deform. Thus, for the purpose of our study, we utilized our 3/10μm asymmetrical design to predict GBM patient outcomes.

Aside from cell migration, cell proliferation is also an important factor that governs cancer aggressiveness and ability to colonize[37]. Ki-67 is a nuclear antigen that is specific to actively proliferating cells and has been used in the clinic to evaluate cancer patient prognosis[38]. With MAqCI, we have the unique ability to assess the proliferative capacities of GBMs, either for the unsorted bulk population or specifically for the sorted highly motile subpopulation. Actively proliferating cells would stain positive for Ki-67 (Fig. 1B). The percentages of Ki-67+ highly motile or unsorted cells were quantified.

A retrospective panel of 28 patient-derived primary GBM cells with complete clinical outcome information was tested in MAqCI in a blind manner to assess their percentages of highly motile cells, narrow entry, highly motile Ki-67+ cells and unsorted Ki-67+ cells. These cells exhibited a heterogeneous and wide range of migratory patterns and proliferative potentials (Fig. 1C). The median survival of this retrospective population was 8.9 months and consisted of 19 patients whom are classified as short-term survivors (<14.6 months, median=5.9 months) and 9 patients whom are classified as long-term survivors (>14.6 months, median=29.3 months) based on the 14.6 months of median GBM patient survival

threshold established by *Stupp et al*[2] (Supplementary Fig. 2A). A list of the relevant and available demographic, tumour, surgical and clinical characteristics for the entire retrospective cohort, as well as the 2 survival subgroups (i.e. short- versus long-term), is available in Supplementary Table 1. Notably, these demographic (age and gender), tumour (pre-operative tumour volume and tumour spread) and surgical attributes (number of surgical resections) all failed to correlate with GBM patient survival (Supplementary Fig. 2B–F). Representative magnetic resonance imaging of the brains of GBM patients reveals a variable degree of tumour size and invasive spread (Supplementary Fig. 2G). Generally, GBM patients with short-term survival possess a larger degree of butterfly tumour spread than long-term survivors, alluding to the potential roles of migration and proliferation as determinants of patient prognosis[4]. However, this pattern was not consistent across our retrospective cohort. Additionally, while the extent of resection and residual tumour volume have correlated with patient prognosis[3], leading surgical teams to aim for gross total resection, pre-operative tumour size has not robustly informed patient outcomes. Given that tumour size is variable during initial presentation at the time of diagnosis, radiographic measures alone cannot be reliably used to predict patient survival. Thus, it is crucial to utilize other measures to accurately evaluate clinical outcomes for each GBM patient.

GBM migration and proliferation correlate with patient survival.

To begin evaluating the prognostic values of the various MAqCI measurement metrics, we separated the retrospective patients into either short- or long-term survival groups and compared their percentages of highly motile cells, narrow entry, highly motile Ki-67+ cells and unsorted Ki-67+ cells. Interestingly, primary GBM cells that are derived from the short-term survivor cohort displayed higher migratory and proliferative potentials, as evidenced by their significantly higher percentage of highly motile Ki-67+ cells (Fig. 2A). The short-term survival group also exhibited a trend of higher percentages of highly motile cells, narrow entry and unsorted Ki-67+ cells (Fig. 2A).

Linear regression between each of the MAqCI measurement metrics and GBM patient survival in months revealed that percentages of highly motile cells, narrow entry and highly motile Ki-67+ cells were all significantly negatively correlated with GBM patient survival (Fig. 2B). Interestingly, there was no significant correlation between percentage of unsorted Ki-67+ cells and GBM patient survival (Fig. 2B).

We next sought to determine a threshold value for each MAqCI measurement metric that can be used to classify the retrospective cohort into either short- or long-term survival groups based on the 14.6 months of median GBM survival threshold established by *Stupp et al*[2]. The individual thresholds used to separate the patients were determined at levels that optimized the sensitivity, specificity, positive predictive value (PPV), negative predictive value (NPV) and accuracy of MAqCI to correctly categorize GBM patients into either short- or long-term survivors (Supplementary Fig. 3A–D). Segmenting the 28 retrospective patients based on the optimal threshold percentages of highly motile cells (3%) or narrow entry (2%) achieved a significant separation of the Kaplan-Meier survival curves, with the curves corresponding to the group exceeding the threshold (high) exhibiting a significantly shorter median survival months than the group that fell below the threshold (low) (Fig. 2C). The

optimal threshold percentage of highly motile Ki-67+ cells (40%) unveiled a trend of separating the survival curves, while the percentage of unsorted Ki-67+ cells (45%), failed to achieve significant survival curve separation (Fig. 2C).

Lastly, receiver-operating characteristic (ROC) curves and their corresponding area under curve (AUC) were generated and calculated for each MAqCI measurement metric to quantify their ability to correctly identify patients based on their actual survival outcomes (Fig. 2D). ROC curve is a graphical representation of the benefit-cost trade-off between the true positive (i.e. sensitivity) and false positive (i.e. 1 minus specificity) of a binary classifier system as its discriminatory threshold is systematically varied. The AUC of ROC indicates the usefulness of a test, where a higher value (with a maximum of 1) corresponds to a more useful test. In addition, the sensitivity, specificity, PPV, NPV and accuracy for each MAqCI measurement metric at their optimal threshold were also tabulated in Table 1. In general, all of the individual MAqCI measurement metrics were able to achieve similar values of around 90% sensitivity and 80% accuracy (Table 1). It is noteworthy that percentage of unsorted Ki-67+ cells represented the most inferior discriminators as compared to the other 3 metrics as it had the lowest value of accuracy (Table 1) and AUC of ROC (Fig. 2D), and did not show any linear correlation to GBM patient survival (Fig. 2B) and significant Kaplan-Meier survival curve separation (Fig. 2C).

Retrospective prediction of GBM patient survival and recurrence.

The percentages of highly motile cells, narrow entry and highly motile Ki-67+ cells correlated to GBM patient survival, but exhibited a rather suboptimal prognostic capability compared to what is considered to be clinically ideal. In order to further improve the predictive power of MAqCI, we combined these 3 indices into a composite MAqCI score (ranging from 0 to 1) using logistic regression (Fig. 3A, Supplementary Table 2). A composite MAqCI threshold score of 0.7 was used to stratify patients into high (>0.7, n=17) and low composite MAqCI score groups (<0.7, n=11) respectively (Supplementary Fig. 3E). The differences in the average composite MAqCI score between the short- and long-term survivors were magnified, with short-term survivors having a significantly higher composite MAqCI score than the long-term survivors (Fig. 3B). The linear correlation between composite MAqCI score and GBM patient survival in months also improved substantially with a noticeably higher R^2 value (Fig. 3C). This classification was able to achieve statistically significant Kaplan-Meier survival curves separation (Fig. 3D). Importantly, the sensitivity, specificity, PPV and accuracy of employing composite MAqCI score to correctly identify short- and long-term survival patients markedly improved to approximately 90% (Table 1). Finally, the AUC of ROC of the composite MAqCI score was also increased to close to 0.90 from around 0.80 for the individual MAqCI measurement metrics, signifying that the composite MAqCI score is a superior binary discriminator than the individual MAqCI measurement metrics (Fig. 3E).

The ability for each individual MAqCI measurement metric and the composite MAqCI score to categorize the 28 retrospective GBM patients into short- versus long-term survival cohorts is summarized in a heat map (Fig. 3F). The numerical individual values behind the heat map classification is provided in Supplementary Table 3. The patient-derived primary GBM lines

were arranged in order of increasing survival and colour coded with a red-blue double gradient with white colour set at the threshold of 14.6 months, while the true red and true blue colours represent the shortest- and longest-term survival, respectively. The effectiveness of the individual MAqCI measurement metrics and the composite MAqCI score were also represented in the red-blue double gradient with white colour being set as the optimal threshold previously determined (i.e. 3% highly motile cells, 2% narrow entry, 40% highly motile Ki-67+ cells, 0.7 composite MAqCI score), and the true red and true blue colour represent the highest and lowest value of each discriminators, respectively. With these heat maps, the false positive (i.e. patients who were long-term survivors, but incorrectly predicted as short-term survivors) and the false negative (i.e. patients who were short-term survivors, but incorrectly predicted as long-term survivors) results were identified by a mismatch in colour hue to the survival heat map panel. The composite MAqCI score emerged as the most accurate binary discriminator compared to the individual MAqCI measurement metrics as it produced the least number of false positive and false negative predictions (Fig. 3F).

In an attempt to achieve a quantitative prediction of survival time, we have also performed a multiple linear regression analysis to generate a semiquantitative correlation between survival months, as treated as a continuous variable, and the various MAqCI measurement metrics. Interestingly, these results matched our findings based on binary classification using logistic regression. Notably, we observed a significant positive correlation between the predicted survival time (as calculated based on the coefficients of multiple linear regression) and actual patient survival time of a R^2 value of 0.41 (Supplementary Fig. 4A–B). While this analysis suggests that MAqCI can provide semiquantitative prediction of survival time for each patient, our data strongly argue for use of a binary classification to inform patient outcomes. However, future development of this technology may provide better quantitative read-outs with increased statistical confidence. Additionally, separating the patient cohort into more than 2 survival groups or creating additional subgroups is challenging because there is no appropriate available clinical or literature guidance to support additional specific survival cut-off points for GBM patients that are meaningful. Along these lines, because less than 5% of GBM patients survive past 5 years[1,2], it is difficult to develop more than 2 clinically meaningful and distinct subgroups.

Notably, the survival prediction made by MAqCI is independent of the demographics, surgical, tumour and clinical attributes of the retrospective patient cohorts. There were no significant differences in terms of age, gender, KPS score, pre-operative tumour volume, extent of resection and tumour extension when the patients are separated based on low versus high MAqCI measurement metrics or composite MAqCI score with their optimized threshold (Supplementary Fig. 5A–F). While IDH1 mutation status has been shown to be an independent prognostic predictor for lower grade gliomas[21], screening of the IDH1 mutation status of our retrospective patient cohort (Supplementary Fig. 6A) revealed its shortcomings in predicting the survival of primary GBM patients. Short- and long-term survivors exhibited a similar incidence of IDH1 mutation (Supplementary Fig. 6B). There was also no difference in terms of mean or median progression-free survival (Supplementary Fig. 6C–D) of GBM patients harbouring wild type or mutated IDH1. With an overall accuracy of only 38% and an AUC of 0.44 (Supplementary Fig. 6E, Table 1), IDH1 mutation status possessed little utility in identifying patients based on their survival outcomes.

To directly compare the performance of MAqCI to that of conventional transwell migration assays for their ability to predict GBM patient survival, we employed the xCELLigence RTCA DP instrument (Acea Biosciences, Inc.) to monitor transwell-migration of our retrospective cohort in CIM-plate 16 chambers. These plates have chambers that are similar to Boyden chambers consisting of an upper chamber where the GBM cells are seeded in serum-free DMEM/F12, a microporous polyethylene terephthalate (PET) membrane with an average pore diameter of 8 μm (through which GBM cells migrate to the lower chamber), electrodes directly below this membrane, and a lower chamber which is filled with DMEM/F12 containing Gem21 Neuroplex supplemented with EGF and FGF as chemoattractants. The extent of GBM cell migration was monitored for 48 h at 15-min intervals by measuring changes in electrical impedance with electrodes that are attached directly underneath the PET membrane. Analysis of the transwell-migration assay revealed a markedly inferior ability to predict patient survival at comparable time scales to our MAqCI assay. Optimization of the sensitivity, specificity and accuracy of the transwell-migration assay by varying the experiment duration and cell index threshold (the readout of cell migration from this instrument) is shown in Supplementary Fig. 7A. At the comparable timescale of MAqCI at 24h, the accuracy and sensitivity of the transwell-migration assay were only 33.3% and 5.6%, respectively (Supplementary Fig. 7B, Table 1). At 24h, most cells demonstrated extremely low levels of migration through transwell (Supplementary Fig. 7C) and the long-term survival groups paradoxically exhibited a slightly higher cell index compared to the short-term survivors (Supplementary Fig. 7D). Nonetheless, there was no significant correlation between GBM patient survival in months (Supplementary Fig. 7E) and Kaplan-Meier survival curve separation when the patients are categorized based on this transwell assay-derived cell index threshold (Supplementary Fig. 7F), resulting in very low AUC of just 0.28 (Supplementary Fig. 7G, Table 1). Taken together, these findings demonstrate the superiority of MAqCI over patient's demographic, surgical, tumour and clinical attributes, IDH1 mutation status and conventional transwell-migration assay to accurately determine the survival outcomes of primary GBM in our retrospective patient cohort.

Aside from GBM patient survival, MAqCI measurement metrics and the composite MAqCI score can also be used to predict time to recurrence. Time to recurrence in months is significantly negatively correlated to percentages of narrow entry and highly motile Ki-67+ cells, and composite MAqCI score, but not percentage of highly motile cells (Fig. 4A). However, GBM lines which were derived from patients with high percentages of highly motile cells, narrow entry and highly motile Ki-67+ cells, and composite MAqCI score all had a significantly shorter time to recurrence (Fig. 4B).

Prospective analysis of GBM patient survival.

To further evaluate the potential for MAqCI to be used in an actual clinical setting for GBM prognosis, we collected and tested in MAqCI specimens from patients from two institutions that we followed prospectively (n=5). For this cohort, the patients were still alive at the time when the *in vitro* experiments and prediction analyses were conducted and hence the survival outcomes were not available to the researchers. We measured the percentages of highly motile cells, narrow entry and highly motile Ki-67+ cells for these 5 prospective

samples and computed the composite MAqCI score (Fig. 4C, Table 2). Only 1 out of the 5 samples (GBM1295) displayed a composite MAqCI score of >0.7 and was predicted to be a short-term survivor, while the other 4 samples (GBM1296, GBM1283, GBM1280 and GBM166) were predicted to be long-term survivors. We continued to follow up with the patients over time and only 1 patient passed away at 14.4 months, before the 14.6 months of median GBM patient survival threshold. That patient is GBM1295, which MAqCI had correctly identified as a short-term survivor (Table 2). The other 4 patients survived past 14.6 months, making them long-term survivors, which MAqCI had also correctly predicted (Table 2). The prognostic performance of MAqCI for the prospective cohort is illustrated in a heat map similar to the retrospective cohort as described earlier (Fig. 3F), where it is evident that the predicted survival outcome based on the composite MAqCI score matches the actual survival outcome for each patient perfectly (Fig. 4D).

Some may argue that the 14.6 months of median survival threshold for GBM as established by Stupp *et al.* might only be applicable for clinical trial participants which is an ideal selected GBM population, and hence may not be ideal to “real world” patients, whom according to Zhu *et al.* exhibit an even shorter median survival time of only 11 months[39]. We chose 14.6 months as our cut-off because our analysis was focused on primary GBM patients, most of whom had undergone standard of care (SOC, surgical resection along with temozolomide and radiation). Unfortunately, the cut-off suggested by Zhu *et al.*, was deemed unsuitable because unlike their study, ours excluded any recurrent patients. Moreover, only a small subset of patients in our study received bevacizumab/Avastin in addition to TMZ and radiotherapy post-debulking, which was a key criterion for the study by Zhu *et al.*.

We noted, however, that 4 out of 28 patients in our retrospective cohort (i.e., 582, 960, 963 and 965) and 2 out of 5 patients in our prospective cohort (i.e., 1280 and 1283) did not receive either temozolomide and/or radiation. Thus, these patients did not receive SOC as stipulated by Stupp *et al.*[2]. To this end, we repeated the analysis for composite MAqCI score, and showed that exclusion of patients who did not receive SOC had a minor effect, if any, on the sensitivity, specificity, PPV, NPV and accuracy of MAqCI in classifying long or short-term survivors relative to the entire patient cohort (Supplementary Table 4). Moreover, inclusion or exclusion of patients who did not receive SOC from the retrospective patient cohort did not alter prediction outcomes and accuracy in the prospective group (Supplementary Table 5). In this study, we generated and utilized cells from resected GBM specimens prior to any treatment exposure. Thus, regardless of any subsequent therapeutic regimens or lack of them, MAqCI is capable of predicting patient outcomes based on GBM aggressiveness using the therapy-naïve cells.

Gene expression profiling of highly motile cell subpopulation.

In view of our data showing correlation between the abundance of highly motile cells and poor patient prognosis, we performed RNA sequencing (RNAseq) to compare the transcriptomes of the highly motile subpopulation versus unsorted bulk cells from two GBM patients with aggressive disease (GBM965 and 897). Based on a quality threshold of RNA Integrity Number (RIN) of ≥8.4, triplicate sample pairs of highly motile and unsorted bulk cell RNA were collected from GBM965 and duplicate pairs from GBM897. Principal

Component Analysis (PCA) identified the inter-tumoral heterogeneity between the samples from the two patients along the first principal component (PC1, $R^2 = 0.99$, $p_{adj} = 6.9e\text{-}13$), which accounted for 63.5% of the variation in the dataset (Fig. 5A, Supplementary Fig. 8B, Supplementary Table 6). The second and third principle components accounted for 6.1% and 5.2% variation, respectively, and did not meaningfully separate the samples by patient or migratory potential ($R^2 < 0.17$) (Supplementary Fig. 8A–B, Supplementary Table 6). Interestingly, the highly migratory versus unsorted bulk cell specimens from both patients separated along the fourth principle component (PC4, $R^2 = 0.67$, $p_{adj} = 0.04$), which accounted for 4.9% of the variation in the dataset (Fig. 5A, Supplementary Table 6). 464 differentially expressed genes (DEGs, FDR<0.1) were identified in highly motile versus bulk unsorted cells from both patients, with 201 DEGs upregulated and 263 downregulated (Fig. 5B, Supplementary Dataset 1). Unsupervised hierarchical clustering of the 10 specimens based on the top 50 statistically significant DEGs separated the specimens by migratory phenotype and then by patient, and showed clusters of conserved gene expression patterns in the highly motile cells (Supplementary Fig. 8C). Gene ontology and biological pathway (GOBP) analyses revealed significant enrichment of biological processes related to cell adhesion, signalling, tissue development/morphogenesis, migration, proliferation, and survival in the highly motile cell population (Fig. 5C, Supplementary Fig. 9A, Supplementary Table 7).

Next, we compared how the gene expression pattern of the highly motile cells was related to the overall survival (OS) of a cohort of 523 GBM patients from The Cancer Genome Atlas program. Of the 464 DEGs identified in the highly motile cells, we found 261 in the microarray data for this cohort. To identify whether patients with high expression of genes upregulated by the migratory cells have a poor prognosis, we calculated a composite score for each patient by summing up the mRNA expression z-score for these DEGs. Patients whose composite scores were above the median value for the cohort were classified as having a high expression of these DEGs. Kaplan Meier survival analysis revealed a trend of reduced OS for upregulated DEGs with p_{adj}=0.1, which reached statistical significance (p=0.035) with a hazard ratio (HR) of 1.22 for the 72 upregulated DEGs with a p_{adj}<0.05 (Fig. 5D) for which expression data were available. Of note, there was no significance in OS for stratifying patients based on downregulated DEGs. We next screened each of the upregulated DEGs identified in the microarray to determine their individual relationship to GBM OS. Stratifying patients based on median gene expression, 20 individual genes significantly (p<0.05) correlated with OS. Importantly, the expression levels of 17 out of the 20 genes (85%) in the highly motile cells relative to the unsorted bulk cell population matched those of GBM patients with short-term survival (Supplementary Table 8). Using the collection of these 17 upregulated DEGs, we calculated a composite score for each patient, and stratified them based on median (Fig. 5E) or tercile (highest third versus lowest third) (Fig. 5F) scores. GBM patients with a high composite score in the expression pattern of these 17 upregulated DEGs had significantly worse OS with a HR of 1.28 (Fig. 5E) and 1.43 (Fig. 5F) for the median and tercile scores, respectively, thereby providing further evidence for the highly motile genotype as an indicator of poor prognosis for GBM patients.

Discussion

The enhanced migratory potential of cancer cells has been linked with higher metastatic propensity, aggressiveness of cancer and overall poor prognosis[40,41] in a variety of cancer types, such as breast and brain[4,31,42,43]. While prior work has revealed that the migratory behaviour of GBM cells is qualitatively instructive in determining tumour aggressiveness[44], no study or method to date has defined an effective quantitative approach for assessing individual patient prognosis for GBM. Moreover, most of our knowledge of cell migration stems from 2D or 3D collagen assays that do not recapitulate the complex *in vivo* brain tissue microenvironment. *In vivo,* invasive GBMs have to navigate and squeeze through confining 3D perivascular tracks in brain vessels formed between glial cells and the basement membrane of vascular smooth muscle cells[45,46]. Prior attempts at examining the relationship between glioma cell migration on 2D surfaces and disease progression have failed to achieve significant predictions to clinically relevant patient features[47]. Introducing complexity to the migration assays by examining the migratory behaviours of individual GBM cells on 1D nano-patterned substratum in response to platelet-derived growth factor (PDGF) stimulation enabled successful prediction of GBM location and recurrence potential in a small retrospective cohort of patients[31]. However, no significant correlation to patient survival outcomes or prognosis was observed[31]. Furthermore, it is unclear whether and how such parameters can independently or in conjunction with other cellular behaviour(s) to quantitatively and precisely predict individual patient clinical outcomes for GBM patients.

In MAqCI, the microchannels were designed to recapitulate key aspects of the complex topography and confining longitudinal pores or perivascular tracks of the brain parenchyma. By examining the migratory behaviours of patient-derived primary GBM cells in response to topographical cues in the absence of any growth factor or chemoattractant stimulation, we found that the percentage of highly motile cells correlates remarkably well with overall progression-free survival. The success of this simple and easy-to-interpret analysis could be attributed to the ability of MAqCI to provide a more physiologically relevant confining microenvironment compared to conventional 1D or 2D migration assays. Along these lines, we also observed significant correlation between patient survival and the percentage of highly motile cells that entered even more confining 3 μm in width branches (i.e., percentage of narrow entry), indicating once again the value of subjecting the cells to migrate in a confined microenvironment and how this phenotypic trait can be exploited to determine patient outcome.

Aside from elevated motility, another key hallmark of aggressive cancer is its ability to grow and proliferate uncontrollably. Ki-67 is a marker that is commonly used in the clinical setting to assess the proliferation potential of cancer biopsies via immunohistochemistry staining and has been explored for cancer prognosis application with variable success[48,49]. However, owing to the inherent heterogeneity of cancer cells, it is challenging to ascertain if migratory and non-migratory cells display distinct proliferative potentials and if these potential differences possess any prognostic values. With MAqCI, we have the unique ability to sort the bulk total cancer cell population into different subpopulations based on their motility and assess their Ki-67 status independently. Notably, if we just quantify the percentage of Ki-67+ cells for the unsorted bulk cell population, similar to just performing

Ki-67 staining without the use of MAqCI, we fail to achieve any correlation to patient survival. In contrast, the percentage of Ki-67+ cells for the highly motile cell subpopulation significantly correlated to GBM patient survival, thereby showcasing the importance of MAqCI as a sorting device. Of note, both metrices were unable to achieve significant survival curve separation, unlike the migratory indices, suggesting that proliferation alone is not sufficient for assessing GBM prognosis despite the promising correlation of highly motile Ki-67+ cells to patient survival.

While individually, migration indices, namely percentages of highly motile cells and narrow entry, and proliferative indices, such as percentage of highly motile Ki-67+ cells, each possesses a certain degree of prognostic value for GBM patients, their independent sensitivity, specificity and accuracy values are not considered clinically ideal. Given that all GBMs exhibit enhanced cellular proliferation, it is difficult to utilize the proliferation index alone as a benchmark for determining individual patient outcomes. It is well established that invasive cells, in order to successfully establish secondary lesions, must proliferate after migrating to the new sites. Therefore, to further improve the prognostic performance of MAqCI, we combined the migratory- and proliferative-based indices using logistic regression into a single composite MAqCI score. Remarkably, the composite MAqCI score emerged as the most accurate predictor compared the individual MAqCI measurement metrics, demonstrating the strongest correlation to patient survival and achieving sensitivity, specificity and accuracy of categorizing patients based on their survival outcomes to close to 90%. Moreover, composite MAqCI score predicts recurrence time successfully in our retrospective patient cohort. Recurrence of GBM following surgical resection represents the primary cause of death in patients and is intimately associated with future patient outcome[3,5]. By quantifying the ability of GBMs to both migrate and proliferate, MAqCI is able to capture this aggressive invasive growth behaviour and capitalize on this knowledge to make meaningful predictions regarding recurrence time and patient survival. Overall, these results reveal the benefits of combining multiple cellular parameters into making accurate prediction related to patient-specific outcomes and prognosis.

Our results also highlight the advantages of MAqCI over traditional non-molecular and molecular characterizations. Notably, demographic, tumour and surgical parameters, such as age, gender, tumour volume, tumour spread, number of surgical resections and KPS score, were all non-indicative of GBM patient survival and prognosis. Interestingly, in our patient cohort, MAqCI outperforms IDH1 mutation status, which is a clinically utilized independent prognosis indicator mainly for low grades gliomas, secondary GBMs, and a subset of primary GBMs. Specifically, in our retrospective patient cohort, we observed no correlation between patient survival and IDH1 mutation status likely due to the limited sample size of the cohort. Thus, MAqCl can inform primary GBM patient prognosis independent of IDH1 mutation status. Furthermore, a direct comparison of the prognostic power of MAqCI and the conventional transwell-migration assay revealed that the latter had a significantly weaker correlation with GBM patient survival. Taken together, we have demonstrated the superior ability of MAqCI to categorize patients based on their individual survival outcomes over other commonly used non-molecular, molecular as well as migration-based assays.

Our retrospective-based findings provided an impetus to further test the efficacy of MAqCI in a prospective manner. As a proof of concept, we collected and tested 5 samples from two different clinical institutions. Out of the 5 prospective patients, only 1 patient passed away before the established median threshold of 14.6 months and was hence classified as a short-term survivor, while the other 4 patients were long-term survivors. Remarkably, MAqCI was able to correctly categorize all 5 patients. This finding suggests the promising potential for MAqCI to be tested in a larger prospective pre-clinical study.

A unique feature of MAqCI is its ability to isolate highly motile cells from a heterogenous tumour cell population for subsequent characterization at the genomic and/or proteomic levels. With the advent of microchannel migration technology capable of extracting phenotypic and molecular parameters of cell invasion[50], it is now feasible to integrate these metrics with transcriptomic or proteomic analyses to further characterize patient-derived GBM cells. To illustrate this capability, we performed RNA sequencing of isolated highly motile relative to unsorted bulk cells from two GBM patients, and determined that upregulated DEGs with a $p_{adj}<0.05$ correlated with poor GBM OS. We also identified a collection of 17 DEGs whose individual expression patterns matched those of GBM patients with reduced overall survival. Importantly, patients with a high composite score based on the expression of these 17 upregulated DEGs displayed reduced OS. Taken together, these findings provide further support for role of highly motile cells in aggressive GBM progression.

Looking forward, MAqCI has the potential to be used in the clinical setting to rapidly distinguish between aggressive and less-aggressive cancers to inform patient care, management, and potential therapies that can impact the disease. During surgical resection of brain cancer, excess tumour specimen, only after allocating a sufficient portion for pathological evaluation and related-standard-of-care examination, can be used to perform MAqCI-related prognostic testing. Importantly, MAqCI technology enables the examination of patient-derived cells from a limited tissue source to quantitatively predict patient cancer aggressiveness. Since we observe a significant positive correlation between the predicted survival time (as calculated based on the coefficients of multiple linear regression) and actual patient survival time, future development of this technology may provide non-binary, quantitative read-outs of survival time with increased statistical confidence for each patient. Moreover, MAqCI can serve as a technology for therapeutic screening to determine individual response and identify patient-specific effective therapies that can reduce the abundance of highly motile and proliferative cells. Given the promising performance of MAqCI in GBM, this functional assay may be useful for determining patient surgical and clinical outcomes of other solid cancers, including those with increased propensity to migrate beyond tumour margins and ultimately metastasize to distal sites. MAqCI can also be extended for basic science applications where in depth molecular and genetic characterizations can be performed on highly motile and/or proliferative cells that can be physically isolated from the device following migration.

Overall, our study reveals that invasive growth is intimately associated with disease progression and overall patient outcomes. By quantitatively evaluating both migratory and proliferative behaviours of patient-derived primary GBM cells in a physiologically relevant

confining microenvironment that mimics the natural invasive routes of native GBM cells, our *in vitro* testing technology, MAqCI, can determine prognosis in a patient-specific manner. We believe that MAqCI technology will provide a useful prognostic tool that can be translated into the clinic to improve personalized management of GBM patients.

Methods

Cells and cell culture.

Patient-derived primary human GBM cells (Retrospective: QNS108, QNS120, GBM153, GBM276, GBM318, GBM496, GBM499, GBM501, GBM549, GBM582, GBM609, GBM612, GBM626, GBM651, GBM653, GBM692, GBM714, GBM724, GBM731, GBM832, GBM847, GBM897, GBM940, GBM960, GBM963, GBM965, GBM1049, GBM1298; Prospective: QNS166, GBM1280, GBM1283, GBM1295, GBM1296) were isolated from primary tumour tissue samples of patients undergoing brain resection surgery for GBM at the Johns Hopkins Hospital and the Mayo Clinic with approval of the Institutional Review Board. Informed patient consent was obtained for both the retrospective and prospective studies. All tumour samples were pathologically confirmed to be GBM. Tissue donors did not receive any treatment prior to surgery. A table summarizing all the demographic, tumour, surgical, and clinical characteristics for each patient in the retrospective and prospective primary GBM cohort is available in Supplementary Table 9. The primary cells were isolated, purified and maintained through previously described methods that eliminate cross-contamination from other cell types and are capable of maintaining the stemness and molecular characteristics of the original primary tumours[51]. The cells were used for no more than 5 passages after they were thawed from the original frozen stock (passage 1–10). The primary GBM cells were grown as adherent cultures on tissue culture flasks pre-coated with laminin (Trevigen) at a density of 1 μg/cm^2 surface area diluted with PBS without magnesium and calcium for 3 h at 37°C. The culture media consisted of 1:1 Dulbecco's Modified Eagle Medium/Nutrient Mixture F-12 (DMEM/F12, Invitrogen), Gem21 Neuroplex™ without vitamin A serum-free supplement (Gemini), 1× antibiotic/antimycotic solution (Sigma-Aldrich), 10 ng/ml of recombinant human fibroblast growth factor (Peprotech) and 20 ng/ml of recombinant human epidermal growth factor (Thermo Fisher Scientific). Accutase solution (Sigma-Aldrich) was used to dissociate cells from the laminin-coated tissue culture flasks instead of trypsin.

Microfluidic Assay for Quantification of Cell Invasion (MAqCI).

MAqCI comprised a series of 400 μm-long and 10 μm-tall Y-shape microchannels[32,33], with a 20 μm-wide feeder channel bifurcating at an angle of 65° to 10 μm-wide or 3 μm-wide branches, arrayed perpendicularly between cell seeding (100 μm-wide, 50 μm-high) and media channels (400μm-wide, 50 μm-high). There is a total of 223 Y-shape microchannels per device spaced at an interval of 50 μm from each other.

MAqCI was fabricated using standard multilayer photolithography and replica moulding techniques[52–54]. The design of the microfluidic device was created in AutoCAD (Autodesk) and transferred to chrome-on-glass darkfield photolithography masks (Photoplot Store). The primary feature of the negative silicon wafer mould, corresponding to the Y-shape

microchannels, was fabricated using SU-8 3010 negative photoresist (Microchem). SU-8 3010 was spun to a thickness of 10 μm on a cleaned silicon wafer (University Wafer) with a spin-coater (Single Wafer Spin Processor, Model WS-400A-6NPP-LITE, Laurell Technologies). The film was soft baked and UV-exposed through a photomask defining the Y-shape microchannels array using an EVG620 mask aligner (EVG) at 170 mJ/cm^2. The exposed wafer was then baked, developed with SU-8 developer, rinsed with isopropanol and dried. To fabricate the cell and medium inlet lines, the photolithography step was repeated using a 50 μm-thick layer of SU-8 3025, with exposure through a mask defining the cells and medium feed lines aligned over primary features at 250 mJ/cm^2. The completed wafer was passivated by treating with (tridecafluoro-1,1,2,2,-tetrahydrooctyl)-1-trichlorosilane (Pfaltz & Bauer) overnight in a vacuum desiccator.

Completed MAqCI was formed using standard replica moulding from the silicon wafer. PDMS elastomer and crosslinker (Sylgard® 184 Silicone Elastomer Kit, Dow Corning) were mixed at a 10:1 w/w ratio, poured over the wafer, degassed in a vacuum, and cured at 85 °C for 2 h. Solidified PDMS were peeled off of the wafer, punched with a 5 mm-diameter hole puncher at the designated well inlets and outlets and cut into appropriate sizes. The cut PDMS devices and 25 mm × 75 mm microscope slides (Electron Microscopy Sciences) were cleaned with 100% ethanol, blown dry with filtered air, and treated with oxygen plasma (Plasma Cleaner PDC-32G, Harrick Plasma) for 2 min at 18W to render the surfaces hydrophilic. The plasma-treated PDMS devices were subsequently attached and sealed to the glass slides. To enable cell binding and adhesion, each MAqCI device was coated with 12 μg/ml of laminin 1 (Trevigen) diluted in PBS without magnesium and calcium at 37 °C for 1 h followed by 4 °C overnight. In select experiments, 20 μg/ml of collagen type I (Thermo Fisher) or 20 μg/ml of fibronectin (Sigma Aldrich) were used to coat MAqCI channels.

MAqCI assay.

Patient-derived primary GBM was detached from laminin-coated tissue culture flask with Accutase, counted and resuspended to a final concentration of 1×10^6 cells/ml. Prior to cell seeding, laminin coating solution was aspirated from the microchannels and the devices were washed once with PBS without magnesium and calcium. Thirty microliters were added to the bottom most medium inlet reservoir as backpressure to prevent the cells from prematurely traversing the Y-shape microchannels by convective flow. Fifty microliters of cell suspension, which is equivalent to 5×10^4 cells, was then introduced to the right cell seeding inlets and the cells were allowed to incubate at 37 °C for 5 min to allow for attachment and seeding at the entrance of the Y-shape microchannels. Afterwards, all cell suspension was transferred from the right to the left cell seeding inlet, and the cells were incubated again for another 5 min. Next, all remaining cells were removed from the cell inlet reservoirs. One hundred microliters of GBM media were then introduced to each of the three medium inlet reservoirs and also the cell seeding inlets on the right side of the device. Migration of GBM in MAqCI was visualized and recorded via time-lapse live microscopy via software-controlled stage automation. The cells were imaged via a 10x/0.30 numerical aperture Ph1 objective lens every 20 min for 24 h using a Digital Sight Qi1Mc camera mounted on a Nikon Inverted microscope equipped with a stage top incubator (Tokai Hit Co., Shizuoka, Japan) maintained at 37°C with 5% CO_2 and humidity.

The video was inspected visually and analysed using the NIS Elements Viewer to quantify the number of highly motile and lowly motile cells. Highly motile cells are defined as cells that migrate up the feeder channels, reach the bifurcation and enter either one of the two branches. Conversely, lowly motile cells include those that enter and migrate in the feeder channels but fail to enter a branch channel. Tracking for a cell ceases either after more than half of the cell body has entered a branch channel or has exited the bottom of the feeder channels. Cells are excluded from analysis if they 1) started already more than half way in the feeder channels at the beginning of the experiment; 2) underwent cell division; 3) exited and re-entered the microchannels in order to avoid double counting. The percentage of highly motile cells was calculated as the ratio of highly motile cells over the sum of both highly motile and lowly motile cells. The number of cells that either entered the 3 μm or and 10 μm-wide branches were also recorded for the calculation of percentage of narrow entry, which is defined as the percentage of highly motile cells that entered the 3 μm narrow channels.

Ki-67 immunofluorescence staining.

Patient-derived primary GBM cells were seeded into MAqCI as per the protocol used for the migration study and allowed to migrate in MAqCI for 24 h at 37°C. Cells were fixed in 4% paraformaldehyde for 20 min, permeabilized in 1% Triton X-100 for 10 min and blocked for 2 h in blocking buffer comprising PBS without magnesium and calcium with 2% bovine serum albumin and 0.1% Triton X-100. Cells were incubated with Ki-67 (8D5) mouse monoclonal antibody (Cell Signaling, 9449S, 1:800) diluted in blocking buffer at 4°C overnight, followed by 2 h incubation with Alexa Fluor 488 goat anti-mouse secondary antibody (Invitrogen, A11001, 1:200) and Hoechst 33342 (Thermo Fisher Scientific, H3570, 1:2000) diluted in blocking buffer at room temperature protected from light. The cells were washed thoroughly with PBS without magnesium and calcium between each step. Imaging of the immunostained samples was performed on an inverted Eclipse Ti epifluorescence microscope (Nikon) with a 10×/0.30 numerical aperture lens. The percentage of Ki-67+ cells was calculated for the highly motile cells (i.e. percentage of highly motile Ki-67+ cells) and for all of the cells that enter the Y-shape microchannels (i.e. percentage of unsorted Ki-67+ cells).

Western blot and antibodies.

Standard western blot techniques were performed as previously described[55]. The antibodies used are listed below. Primary antibodies: 1) IDH1 (D2H1) rabbit mouse monoclonal antibody (Cell Signaling, 8137S, 1:1000). 2) Anti-IDH1 R132H mouse monoclonal antibody (Sigma Aldrich, SAB4200548, 1:250). 3) GAPDH (14C10) rabbit monoclonal antibody (Cell Signaling, 2118S, 1:2000). Secondary antibodies: 1) Anti-mouse IgG, HRP-linked antibody (Cell Signaling, 7076S, 1:2000). 2) Anti-rabbit IgG, HRP-linked antibody (Cell Signaling, 7074S, 1:2000).

Transwell-migration assay.

Transwell-migration of the retrospective patient-derived primary cells were monitored using the xCELLigence RTCA DP instrument (Acea Biosciences, Inc.) according to the manufacturer's protocol using a CIM-plate 16 chambers[32]. These plates have chambers that

are similar to Boyden chambers; they consist of an upper chamber where the GBM cells are seeded in serum-free DMEM/F12, a microporous polyethylene terephthalate (PET) membrane with an average pore diameter of 8 μm (through which GBM cells migrate to the lower chamber), electrodes directly below this membrane, and a lower chamber which is filled with DMEM/F12 containing Gem21 Neuroplex supplemented with EGF and FGF as chemoattractant. 4×10^4 cells per well were seeded into the upper chamber of a CIM-plate 16 chambers. The extent of GBM cell migration was monitored in real time as cell index for 48 h at 15 min intervals in a humidified incubator maintained at 37 °C and 5% CO_2 by measuring changes in electrical impedance with electrodes that are attached directly underneath the PET membrane. Each patient-derived primary GBM specimen was run in triplicate for each experiment.

Correlation between *in vitro* MAqCI and clinical data.

To assess the relationship between the migratory and proliferative measurements obtained with MAqCI to clinical patient outcome, the samples were separated into short- and long-term survival groups based on the threshold of 14.6 month of median GBM patient survival established by Stupp et al.[2]. Student's t-test was conducted to detect statistical difference between the MAqCI measurement metrics between the short- versus long-term survival groups. Additionally, Pearson's correlation analysis was conducted to assess the linear correlation between the MAqCI measurement metrics and patient survivals (in months).

Identification of optimal threshold.

The thresholds of the *in vitro* MAqCI measurement metrics were systematically varied. For each threshold value, the percentage of the *in vitro* MAqCI measurement metric was compared against to classify the samples into either long-term survivors (< threshold) or short-term survivors (≥threshold). MAqCI's prediction was then compared to the actual patient survival months which have been previously stratified into short- and long-term survivors based on the 14.6 months median GBM patient survival established by Stupp et al[2], to label each prediction as true positive, true negative, false positive, or false negative (where true represents a match between MAqCI's prediction and actual patient survival, and positive/negative denotes short- or long-term survivors, respectively). With these classifications, the prediction performance characteristics, including sensitivity, specific, PPV, NPV and accuracy, of the MAqCI measurement metrics at that particular threshold value were computed. This process was iterated for the entire range of each MAqCI measurement metric and the optimal threshold value was selected at a value that maximized the average of all the prediction performance characteristics.

Assessment of the prognostic value of MAqCI measurement metrics.

The patient survival data was plotted as a Kaplan-Meier graph and the mean survival time in months of patients were compared between the groups separated by the optimal threshold determined. Log-Rank (Mantel Cox) test was conducted to detect statistical significance between the two survival curves. The performance characteristics, including sensitivity, specificity, PPV, NPV, accuracy and area under curves of receiver operating characteristic curve, of each of the MAqCI measurement metric in successfully classifying patients into either short- or long-term survivors was computed and tabulated. Additionally, the time to

recurrence of the samples was compared between groups as separated by the optimal threshold. Similar Kaplan-Meier curve comparisons were also made with demographic, surgical and tumour characteristic information collected from the patients to assess the prognostic values of these other clinically available indices.

Logistic Regression.

A composite MAqCI score that combines the individual MAqCI measurement metrics was computed via logistic regression, where the probability of each sample belonging to the short-term survival group (i.e., <14.6 months) was calculated based on the predictors (X_i): percentage of highly motile cells, percentage of narrow entry and percentage of highly motile Ki-67+ cells, Equation (1). Logistic regression coefficients (b_i) were determined in MATLAB using the glmfit function for all the retrospective cell lines (n=28) based on the short- and long-term GBM survival stratification of 14.6 months (Supplementary Table 2). Probability values, namely composite MAqCI scores, were calculated in MATLAB using the glmfit function. Similar threshold identification, correlation and Kaplan-Meier curve comparison analyses as described above were repeated with the composite MAqCI score to evaluate its prognostic performance.

$$p = \frac{e^{(b_0 + b_1 X_1 + b_2 X_2 + b_3 X_3)}}{1 + e^{(b_0 + b_1 X_1 + b_2 X_2 + b_3 X_3)}} \quad \text{Equation (1)}$$

Isolation of highly motile cells.

Approximately 5×10^4 patient-derived primary GBM cells (specifically GBM897 and GBM965) were seeded in MAqCI and allowed to travel through the microchannels for 48 h. Highly motile cells that have successfully exited the branch channels and entered the collection channel were first washed with PBS and then dissociated from the device with TrypLE Express reagent (Gibco) for 10 min. A microbore tubing connected to a 10 ml syringe filled with regular GBM culture media was attached to a collection inlet. Pressure was then applied to push the media from the syringe through the collection channel to force the detached highly motile cells into the collection outlet. These cells were subsequently collected with a micropipette and transferred to a 15ml tube with 2ml of regular GBM culture media. Typically, each MAqCI device produced around 50–100 highly motile cells. Highly motile cells from multiple MAqCI were pooled to yield a greater number of cells for downstream processing for RNAseq. Similar procedures were repeated for cells seeded in the cell seeding channels to obtain an unsorted bulk population as control. The number of unsorted cells were normalized and diluted accordingly to the number of isolated highly motile cells, as enumerated manually during the isolation process by microscope observation.

RNAseq and analysis.

Total RNA was purified from equal numbers of highly motile or unsorted bulk cells using the RNeasy Micro Kit (Qiagen). RNA was evaluated by Bioanalyzer using the Agilent RNA 60000 Pico kit. Samples with an RNA Integrity Number (RIN) of 8.4–9.3 were used. 335 pg

of RNA of each sample were used to prepare complementary DNA (cDNA) libraries using the Smart-seq v4 kit (Takara). cDNAs were purified by AMPure XP beads, fragmented by sonication to ~400bp, and subjected to barcoding and single-end sequenced on an Illumina NextSeq 500 with 75 cycles. RNA-seq reads were mapped to hg38 reference genome using HISAT2[56] aligner. HTSeq framework[57] was used to quantify read counts per gene from aligned reads using human GENCODE release 33 (GRCh38.p13) gene models. The Bioconductor/R packages DESeq2_1.26.0[58] was used for normalization and differential gene expression analysis. Principal component analysis was performed on regularized logarithm (rlog) transformed counts. GO term enrichment analysis was performed using GOrilla database[59,60].

Survival analysis based on patient gene expression pattern.

Patient survival and gene expression data for 12,042 unique genes based on microarray analysis from the TCGA Firehose Legacy cohort were downloaded from cBioPortal. Using a custom MATLAB code, each patient's z-score for each upregulated DEG of interest was summed up to create a composite score for that patient. Patients with composite scores above the median composite score for the cohort were classified as having high expression. For select analyses, the upper and lower tercile of composite scores were used to stratify the patients instead of the median. The code then tabulated the survival data for patients in both groups. Then, GraphPad Prism was used to generate Kaplan-Meier survival plots, log-rank statistical tests, hazard ratios and 95% confidence intervals of the hazard ratios.

Statistical analysis.

All data are presented as mean±S.E.M. from n≥3 independent biological replicates unless otherwise stated. Graphing and statistical analyses were performed with GraphPad Prism 7 (Graphpad Software). Statistical significance was determined between pairs of data with an unpaired student's t-test for continuous variables and Fisher's exact test for categorical variables. Pearson's correlation was used to assess the degree of correlation between two continuous variables. Two-tailed log-rank (Mantel-Cox) test was employed to assess the statistical difference between two Kaplan-Meier survivor curves. For principal component correlation analysis, a two-tailed t-test was performed for Pearson's correlation coefficient R, which follows a t-distribution with $n\text{-}2$ degrees of freedom as described by Equation (2).

$$t = \frac{R\sqrt{n-2}}{\sqrt{1-R^2}\Big)} \qquad \text{Equation (2)}$$

Reporting summary.

Further information on research design is available in the Nature Research Reporting Summary linked to this article.

Data availability

The main data supporting the results in this study are available within the paper and its Supplementary Information. The raw and analysed datasets generated during the study are too large to be publicly shared, yet they are available for research purposes from the corresponding authors on reasonable request. RNA sequencing data are available at the National Center for Biotechnology Information Gene Expression Omnibus under accession number GSE144610.

Supplementary Material

Refer to Web version on PubMed Central for supplementary material.

Acknowledgements

This line of research was supported by the National Cancer Institute through grants R01-CA216855 (A.Q.H. and K.K.), R01-CA183804 (K.K.) and R01-CA124704 (S.S.M.) and a Department of Defence grant CA160997 (V.K.B.). A.Q.H. was also supported by the Mayo Clinic Clinician Investigator Award and the William J. and Charles H. Mayo Professorship.

References

1. Ostrom QT et al. CBTRUS Statistical Report: Primary Brain and Other Central Nervous System Tumors Diagnosed in the United States in 2011–2015. Neuro Oncol 20, iv1–iv86 (2018). [PubMed: 30445539]
2. Stupp R. et al. Radiotherapy plus concomitant and adjuvant temozolomide for glioblastoma. N Engl J Med 352, 987–996 (2005). [PubMed: 15758009]
3. Chaichana KL et al. Establishing percent resection and residual volume thresholds affecting survival and recurrence for patients with newly diagnosed intracranial glioblastoma. Neuro Oncol 16, 113–122 (2014). [PubMed: 24285550]
4. Shah SR et al. YAP controls cell migration and invasion through a Rho-GTPase switch. bioRxiv, 602052 (2019).
5. Chaichana KL et al. Multiple resections for patients with glioblastoma: prolonging survival. J Neurosurg 118, 812–820 (2013). [PubMed: 23082884]
6. Chaichana K, Parker S, Olivi A & Quinones-Hinojosa A. A proposed classification system that projects outcomes based on preoperative variables for adult patients with glioblastoma multiforme. J Neurosurg 112, 997–1004 (2010). [PubMed: 19817542]
7. Wei S. et al. Heterozygous IDH1(R132H/WT) created by “single base editing” inhibits human astroglial cell growth by downregulating YAP. Oncogene 37, 5160–5174 (2018). [PubMed: 29849122]
8. Grossman R. et al. MGMT inactivation and clinical response in newly diagnosed GBM patients treated with Gliadel. J Clin Neurosci 22, 1938–1942 (2015). [PubMed: 26249244]
9. Parsons DW et al. An integrated genomic analysis of human glioblastoma multiforme. Science 321, 1807–1812 (2008). [PubMed: 18772396]
10. Brennan CW et al. The somatic genomic landscape of glioblastoma. Cell 155, 462–477 (2013). [PubMed: 24120142]
11. Noushmehr H. et al. Identification of a CpG island methylator phenotype that defines a distinct subgroup of glioma. Cancer Cell 17, 510–522 (2010). [PubMed: 20399149]
12. Phillips HS et al. Molecular subclasses of high-grade glioma predict prognosis, delineate a pattern of disease progression, and resemble stages in neurogenesis. Cancer Cell 9, 157–173 (2006). [PubMed: 16530701]

13. Verhaak RG et al. Integrated genomic analysis identifies clinically relevant subtypes of glioblastoma characterized by abnormalities in PDGFRA, IDH1, EGFR, and NF1. Cancer Cell 17, 98–110 (2010). [PubMed: 20129251]
14. Colman H & Aldape K. Molecular predictors in glioblastoma: toward personalized therapy. Arch Neurol 65, 877–883 (2008). [PubMed: 18625854]
15. Jaeckle KA et al. Correlation of tumor O6 methylguanine-DNA methyltransferase levels with survival of malignant astrocytoma patients treated with bis-chloroethylnitrosourea: a Southwest Oncology Group study. J Clin Oncol 16, 3310–3315 (1998). [PubMed: 9779706]
16. Hegi ME et al. Clinical trial substantiates the predictive value of O-6-methylguanine-DNA methyltransferase promoter methylation in glioblastoma patients treated with temozolomide. Clin Cancer Res 10, 1871–1874 (2004). [PubMed: 15041700]
17. Hegi ME et al. MGMT gene silencing and benefit from temozolomide in glioblastoma. N Engl J Med 352, 997–1003 (2005). [PubMed: 15758010]
18. Shah SR, Q.-H. A, Xia S. Advances in Brain Cancer: Creating Monoallelic Single Point Mutation in IDH1 by Single Base Editing. Journal of Oncology Research and Therapy 05, 1–3 (2018).
19. Preusser M. et al. Anti-O6-methylguanine-methyltransferase (MGMT) immunohistochemistry in glioblastoma multiforme: observer variability and lack of association with patient survival impede its use as clinical biomarker. Brain Pathol 18, 520–532 (2008). [PubMed: 18400046]
20. Grasbon-Frodl EM et al. Intratumoral homogeneity of MGMT promoter hypermethylation as demonstrated in serial stereotactic specimens from anaplastic astrocytomas and glioblastomas. Int J Cancer 121, 2458–2464 (2007). [PubMed: 17691113]
21. Hartmann C. et al. Type and frequency of IDH1 and IDH2 mutations are related to astrocytic and oligodendroglial differentiation and age: a study of 1,010 diffuse gliomas. Acta Neuropathol 118, 469–474 (2009). [PubMed: 19554337]
22. Yan H. et al. IDH1 and IDH2 mutations in gliomas. N Engl J Med 360, 765–773 (2009). [PubMed: 19228619]
23. Cancer Genome Atlas Research, N. et al. Comprehensive, Integrative Genomic Analysis of Diffuse Lower-Grade Gliomas. N Engl J Med 372, 2481–2498 (2015). [PubMed: 26061751]
24. Eckel-Passow JE et al. Glioma Groups Based on 1p/19q, IDH, and TERT Promoter Mutations in Tumors. N Engl J Med 372, 2499–2508 (2015). [PubMed: 26061753]
25. Joo KM et al. Patient-specific orthotopic glioblastoma xenograft models recapitulate the histopathology and biology of human glioblastomas in situ. Cell Rep 3, 260–273 (2013). [PubMed: 23333277]
26. Specht H & Slavov N. Transformative Opportunities for Single-Cell Proteomics. J Proteome Res 17, 2565–2571 (2018). [PubMed: 29945450]
27. Wills QF & Mead AJ Application of single-cell genomics in cancer: promise and challenges. Hum Mol Genet 24, R74–84 (2015). [PubMed: 26113645]
28. Chandler Y. et al. Cost Effectiveness of Gene Expression Profile Testing in Community Practice. J Clin Oncol 36, 554–562 (2018). [PubMed: 29309250]
29. Lippman M & Osborne CK Circulating tumor DNA--ready for prime time? N Engl J Med 368, 1249–1250 (2013). [PubMed: 23484798]
30. Smith CL et al. Pre-exposure of human adipose mesenchymal stem cells to soluble factors enhances their homing to brain cancer. Stem Cells Transl Med 4, 239–251 (2015). [PubMed: 25646527]
31. Smith CL et al. Migration Phenotype of Brain-Cancer Cells Predicts Patient Outcomes. Cell Rep 15, 2616–2624 (2016). [PubMed: 27292647]
32. Yankaskas CL et al. A microfluidic assay for the quantification of the metastatic propensity of breast cancer specimens. Nat Biomed Eng 3, 452–465 (2019). [PubMed: 31061459]
33. Paul CD et al. Interplay of the physical microenvironment, contact guidance, and intracellular signaling in cell decision making. FASEB J 30, 2161–2170 (2016). [PubMed: 26902610]
34. Wolf K. et al. Collagen-based cell migration models in vitro and in vivo. Semin Cell Dev Biol 20, 931–941 (2009). [PubMed: 19682592]

35. Jucker M, Tian M & Ingram DK Laminins in the adult and aged brain. Mol Chem Neuropathol 28, 209–218 (1996). [PubMed: 8871961]
36. Weigelin B, Bakker GJ & Friedl P. Intravital third harmonic generation microscopy of collective melanoma cell invasion: Principles of interface guidance and microvesicle dynamics. Intravital 1, 32–43 (2012). [PubMed: 29607252]
37. Xie Q, Mittal S & Berens ME Targeting adaptive glioblastoma: an overview of proliferation and invasion. Neuro Oncol 16, 1575–1584 (2014). [PubMed: 25082799]
38. Inwald EC et al. Ki-67 is a prognostic parameter in breast cancer patients: results of a large population-based cohort of a cancer registry. Breast Cancer Res Tr 139, 539–552 (2013).
39. Zhu P, Du XL, Lu G & Zhu JJ Survival benefit of glioblastoma patients after FDA approval of temozolomide concomitant with radiation and bevacizumab: A population-based study. Oncotarget 8, 44015–44031 (2017). [PubMed: 28467795]
40. Steeg PS Targeting metastasis. Nat Rev Cancer 16, 201–218 (2016). [PubMed: 27009393]
41. Paul CD, Mistriotis P & Konstantopoulos K. Cancer cell motility: lessons from migration in confined spaces. Nat Rev Cancer 17, 131–140 (2017). [PubMed: 27909339]
42. Liu JC, Zacksenhouse M, Eisen A, Nofech-Mozes S & Zacksenhaus E. Identification of cell proliferation, immune response and cell migration as critical pathways in a prognostic signature for HER2+:ERalpha- breast cancer. PLoS One 12, e0179 (2017).
43. Shah SR et al. 217 YAP Is Ready to Rac and Rho: Elucidation of a Novel YAP-Driven Network That Potentiates Brain Cancer Cell Dispersal and Confers Poor Survival in Patients. Neurosurgery 63, 185–185 (2016).
44. Armento A, Ehlers J, Schotterl S & Naumann U in Glioblastoma (ed De Vleeschouwer S) (2017).
45. Gritsenko P, Leenders W & Friedl P. Recapitulating in vivo-like plasticity of glioma cell invasion along blood vessels and in astrocyte-rich stroma. Histochem Cell Biol 148, 395–406 (2017). [PubMed: 28825130]
46. Friedl P & Alexander S. Cancer invasion and the microenvironment: plasticity and reciprocity. Cell 147, 992–1009 (2011). [PubMed: 22118458]
47. Friedlander DR et al. Migration of brain tumor cells on extracellular matrix proteins in vitro correlates with tumor type and grade and involves alphaV and beta1 integrins. Cancer Res 56, 1939–1947 (1996). [PubMed: 8620517]
48. Wong E. et al. Cut-point for Ki-67 proliferation index as a prognostic marker for glioblastoma. Asia Pac J Clin Oncol 15, 5–9 (2019).
49. Abubakar M. et al. Prognostic value of automated KI67 scoring in breast cancer: a centralised evaluation of 8088 patients from 10 study groups. Breast Cancer Research 18 (2016).
50. Lin JG et al. Linking invasive motility to protein expression in single tumor cells. Lab Chip 18, 371–384 (2018). [PubMed: 29299576]
51. Shah SR et al. Brachyury-YAP Regulatory Axis Drives Stemness and Growth in Cancer. Cell Rep 21, 495–507 (2017). [PubMed: 29020634]
52. Mistriotis P. et al. Confinement hinders motility by inducing RhoA-mediated nuclear influx, volume expansion, and blebbing. J Cell Biol 218, 4093–4111 (2019). [PubMed: 31690619]
53. Tong Z. et al. Chemotaxis of cell populations through confined spaces at single-cell resolution. PLoS One 7, e29211 (2012).
54. Zhao R. et al. Cell Sensing and Decision-Making in Confinement: The role of TRPM7 in a tug of war between hydraulic pressure and cross-sectional area. Science Advances 5, eaaw7243 (2019).
55. Chen SH, Hung WC, Wang P, Paul C & Konstantopoulos K. Mesothelin binding to CA125/MUC16 promotes pancreatic cancer cell motility and invasion via MMP-7 activation. Sci Rep 3, 1870 (2013). [PubMed: 23694968]
56. Kim D, Langmead B & Salzberg SL HISAT: a fast spliced aligner with low memory requirements. Nat Methods 12, 357–360 (2015). [PubMed: 25751142]
57. Anders S, Pyl PT & Huber W. HTSeq--a Python framework to work with high-throughput sequencing data. Bioinformatics 31, 166–169 (2015). [PubMed: 25260700]
58. Love MI, Huber W & Anders S. Moderated estimation of fold change and dispersion for RNA-seq data with DESeq2. Genome Biol 15, 550 (2014). [PubMed: 25516281]

59. Eden E, Navon R, Steinfeld I, Lipson D & Yakhini Z. GOrilla: a tool for discovery and visualization of enriched GO terms in ranked gene lists. BMC Bioinformatics 10, 48 (2009). [PubMed: 19192299]

60. Eden E, Lipson D, Yogev S & Yakhini Z. Discovering motifs in ranked lists of DNA sequences. PLoS Comput Biol 3, e39 (2007).

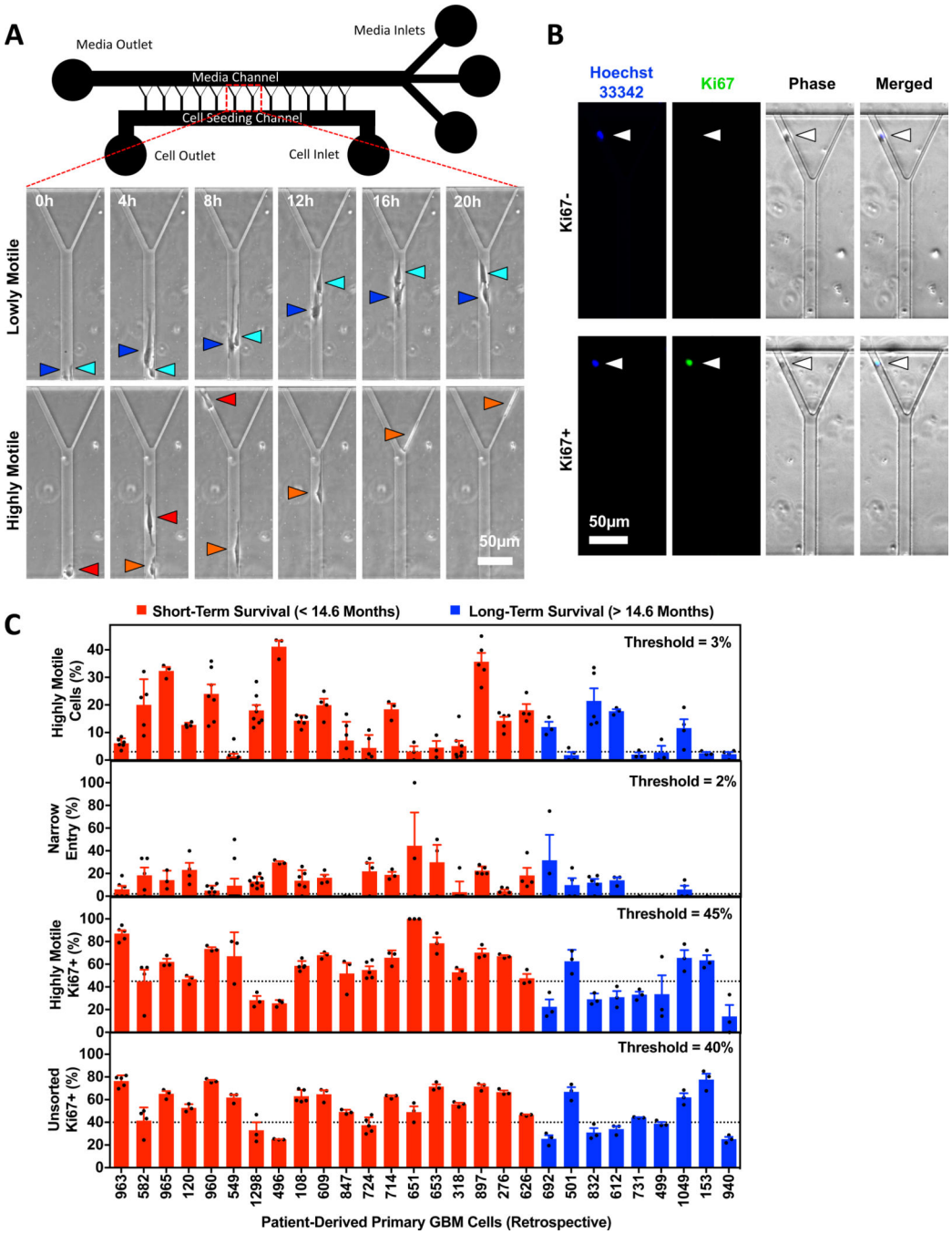

Fig. 1 |. Microfluidic Assay for Quantification of Cell Invasion (MAqCI) distinguishes patient-derived primary GBM cells based on their migratory and proliferative potentials.

(A) Schematic of MAqCI consisting of a series of 10 μm-tall and 400 μm-long Y-shape microchannels, with a 20 μm-wide feeder channel bifurcating to either a 10 μm- or 3 μm-wide branches. Inset: Representative time-lapse micrographs of GBM714 migrating in MAqCI. Lowly motile cells (top row) are defined as cells that remain in the feeder channels and fail to enter the bifurcations (blue and cyan triangles). Highly motile cells (bottom row) are defined as cells that traverse through the entire length of the feeder channel and enter

either the 10 μm wide (red triangle) or 3 μm narrow branches (orange triangle). Duration between each frame is 4 h. The representative images were selected from time-lapse migration videos of GBM migrating in MAqCI, which typically consists of 4 to 5 Y-shape microchannels per field of view for a total of 223 microchannels, amounting to a total of 46 to 56 fields of view per MAqCI device. For each cell line, at least 3 biological replicates were performed. Thus, at least 650 individual Y-shape microchannels were imaged per cell line. **(B)** Representative epifluorescence images of Ki-67-negative non-proliferative (top row) and Ki-67+ proliferative (bottom row) GBM965 that have migrated in MAqCI. The cells (white triangles) were immunostained for Ki-67 (green) and counterstained for nucleus with Hoechst 33342 (blue). The representative images were selected from epifluorescences images of immunolabeled GBM cells in MAqCI. At least 650 individual Y-shape microchannels (see above) were imaged per cell line. **(C)** Percentage of highly motile cells (1^{st} row), percentage of narrow entry (2^{nd} row), percentage of highly motile Ki-67+ cells (3^{rd} row) and percentage of unsorted Ki-67+ cells (4^{th} row) for a retrospective panel of 28 patient-derived primary GBM cells tested with MAqCI. Red bars represent cells that are derived from patients with short-term survival (<14.6 months, n=19). Blue bars represent cells that are derived from patients with long-term survival (>14.6 months, n=9). Data represent the mean±S.E.M. from n≥3 biological replicates.

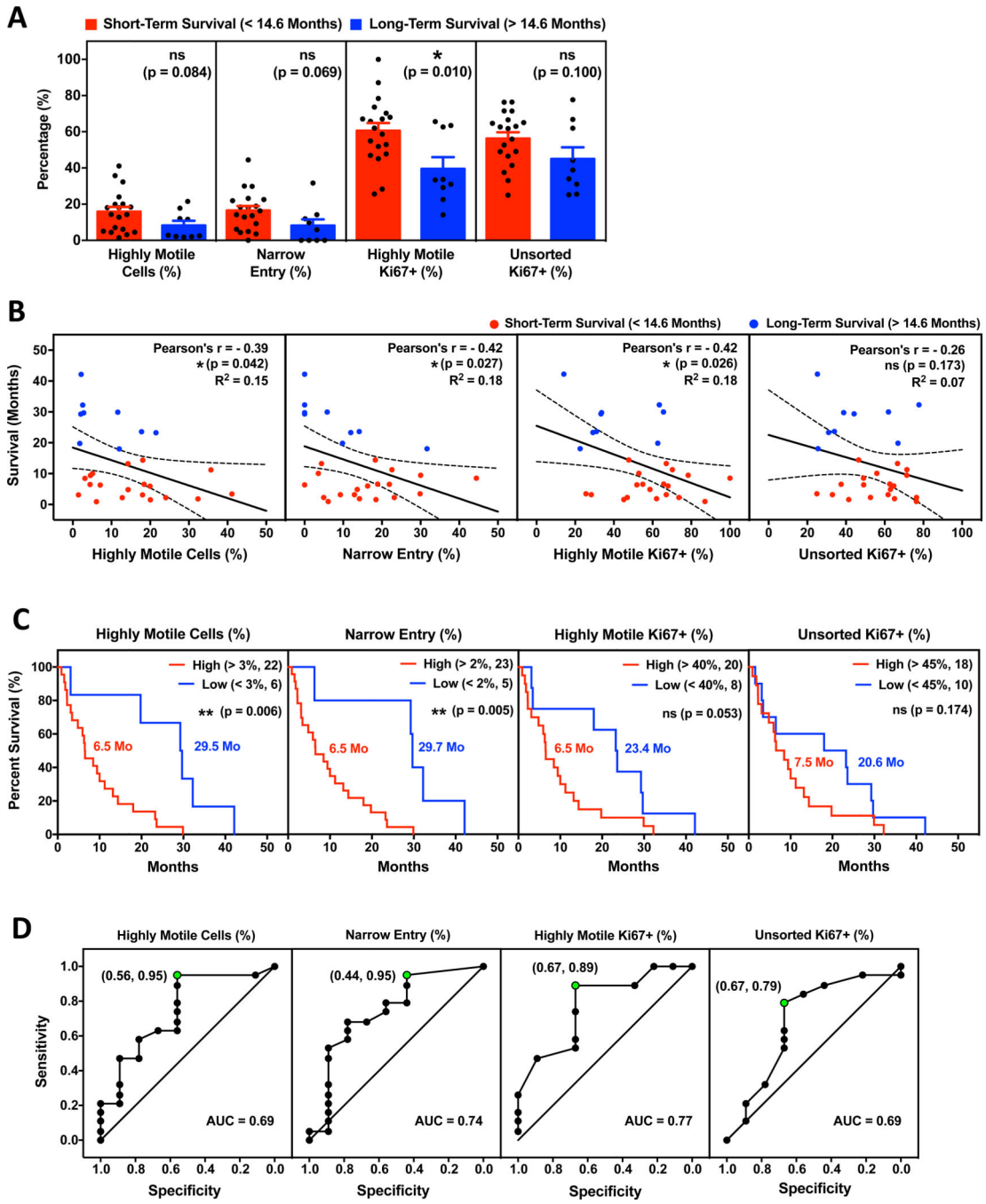

Fig. 2 |. GBM migratory and proliferative potentials correlate with patient survival.

(A) The retrospective GBM patient cohort is separated into short- (red bars, n=19) and long-term survivors (blue bars, n=9), and compared for their average percentages of highly motile cells (1st panel), narrow entry (2nd panel), highly motile Ki-67+ cells (3rd panel) and unsorted Ki-67+ cells (4th panel). * represents $p<0.05$ as assessed by unpaired student's t-test. **(B)** Linear regression analysis of GBM patient survival in months against percentages of highly motile cells (1st panel), narrow entry (2nd panel), highly motile Ki-67+ cells (3rd panel) and unsorted Ki-67+ cells (4th panel). Black solid line represents the best-fit line

while black dotted lines represent the 95% confidence interval. * represents $p<0.05$. Pearson's correlation was used to assess the significance of the correlation. **(C)** Kaplan-Meier curves based on MAqCI measurements, comparing survival of the retrospective cohort as separated by percentages of highly motile cells (1st panel), narrow entry (2nd panel), highly motile Ki-67+ cells (3rd panel) and unsorted Ki-67+ cells (4th panel). ** represents $p<0.01$ and ns represents $p>0.05$ as assessed by two-tailed log-rank (Mantel-Cox) test. **(D)** Receiver operating characteristic curves of classifying GBM patients into short- or long-term survivors based on percentages of highly motile cells (1st panel), narrow entry (2nd panel), highly motile Ki-67+ cells (3rd panel) and unsorted Ki-67+ cells (4th panel). Area under curve (AUC) was calculated to indicate the prognostic utility of the different classifiers.

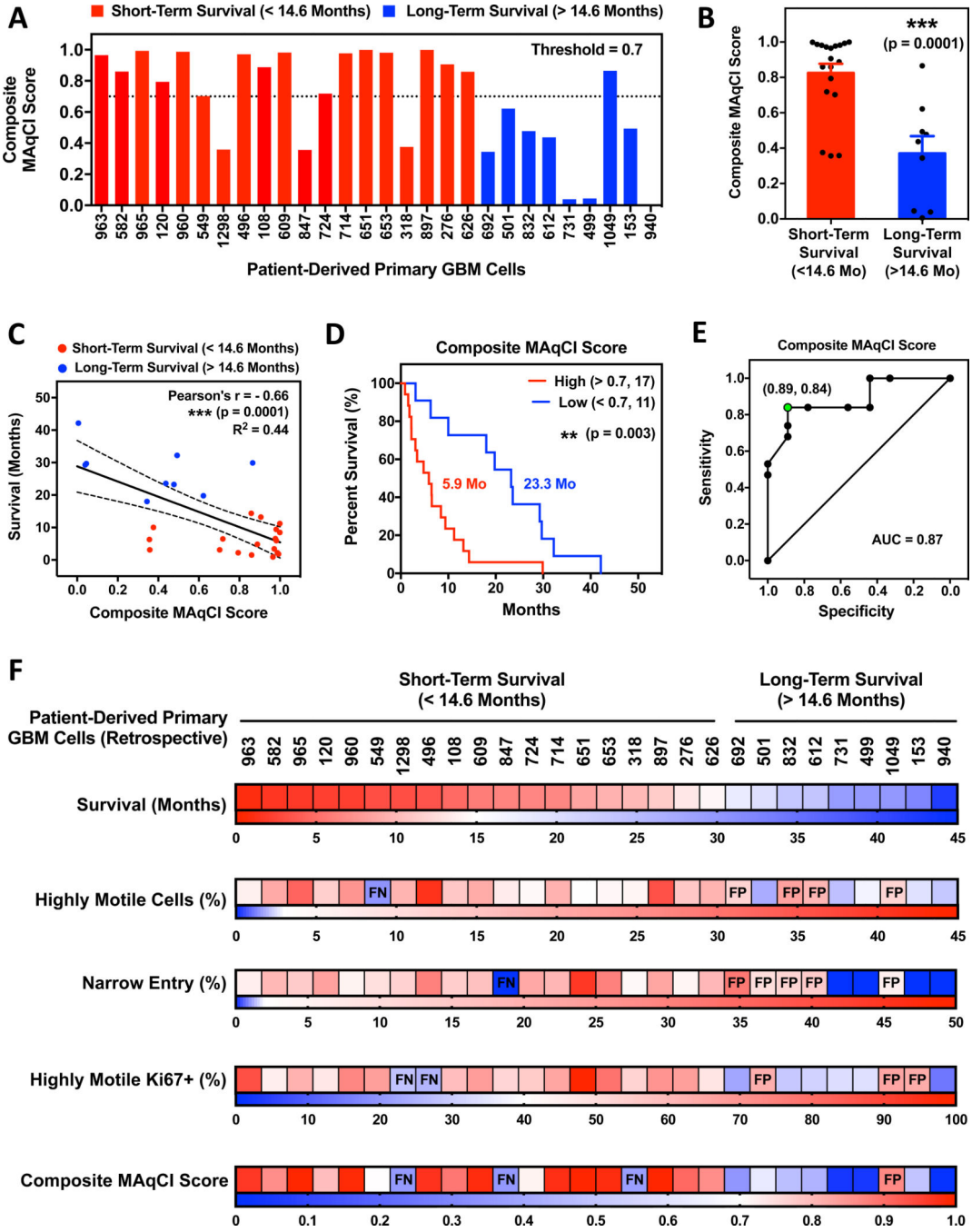

Fig. 3 |. Combining migratory and proliferative indices into a single composite score maximizes the prognostic performance of MAqCI.

(A) The values of composite MAqCI score computed with logistic regression by combining percentages of highly motile cells, narrow entry and highly motile Ki-67+ cells as independent predictors. **(B)** Mean composite MAqCI score of short- (red bar, n=19) versus long-term (blue bar, n=9) survivors. *** represents p<0.001 as assessed by unpaired student's t-test. **(C)** Linear regression analysis of GBM patient survival against composite MAqCI score. Black solid line represents the best-fit line while black dotted lines represent

the 95% confidence interval. *** represents p<0.001. Pearson's correlation was used to assess the significance of the correlation. **(D)** Kaplan-Meier curve based on composite MAqCI score, comparing survival of the retrospective cohort as separated by high (>0.7, n=17) or low (<0.5, n=11) composite MAqCI score. ** represents p<0.01 as assessed by two-tailed log-rank (Mantel-Cox) test. **(E)** Receiver operating characteristic curve of classifying GBM patients into short- or long-term survivors based on composite MAqCI score. AUC was calculated to indicate the prognostic utility of composite MAqCI score in classifying GBM patient into short- or long-term survivals. **(F)** Heat maps summarizing the ability of individual MAqCI measurement metrics and composite MAqCI score in categorizing GBM patients into short- or long-term survivors. The 28 GBM patients are arranged in increasing order with survival (1st panel), percentage of highly motile cells (2nd panel), percentage of narrow entry (3rd panel) and percentage of highly motile Ki-67+ cells (4th panel) and composite MAqCI score (5th panel) of the 28 retrospective GBM patients as presented in a red-blue double gradient with white colour set as the threshold. False positive (FP: patients who are incorrectly categorized as short-term survivors) and false negative (FN: patients who are incorrectly categorized as long-term survivors) are indicated.

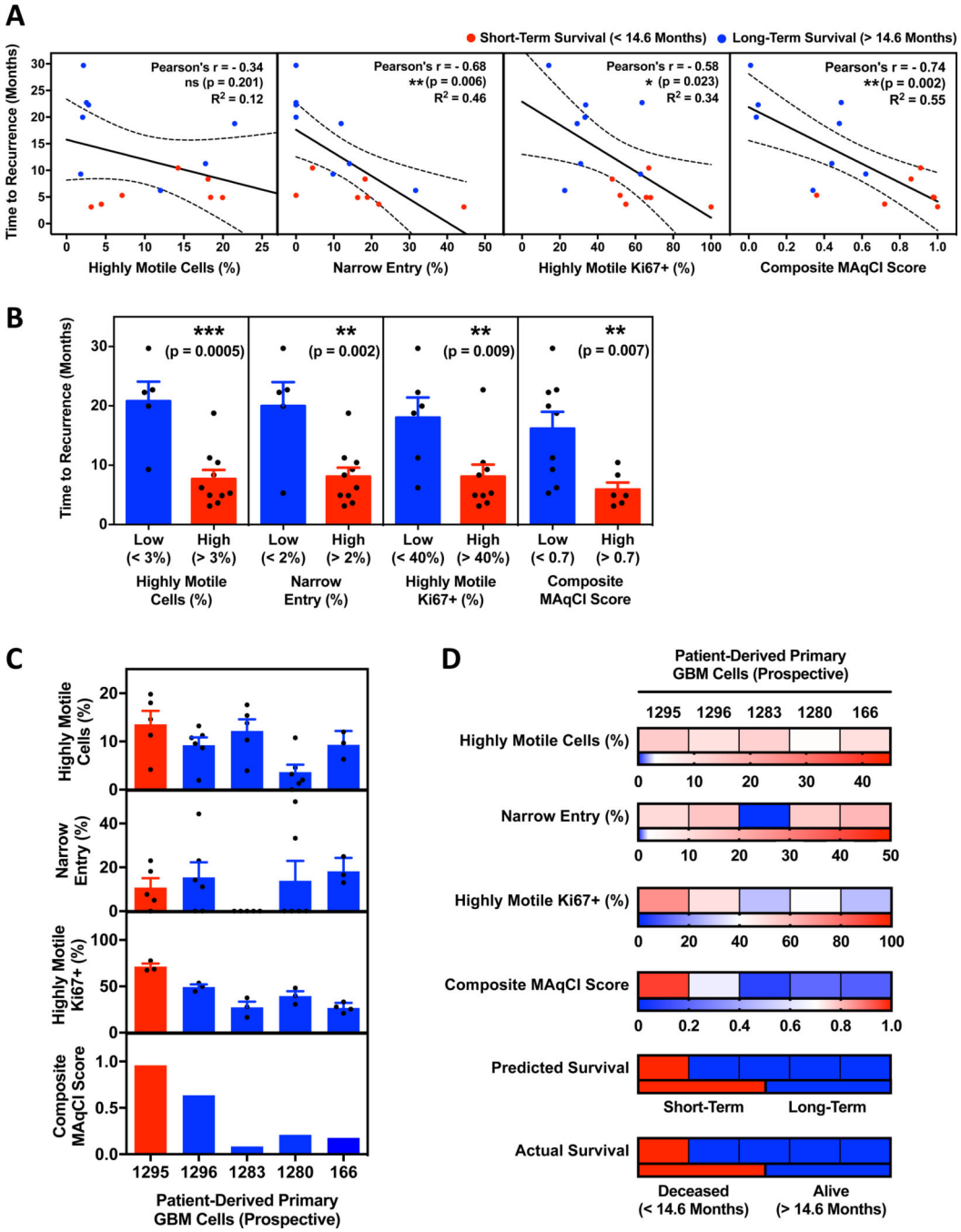

Fig. 4 |. MAqCI predicts recurrence time in a retrospective cohort and correctly categorizes GBM patients based on progression-free survival prospectively.

(A) Linear regression analysis of GBM patient time to recurrence in months against percentages of highly motile cells (1st panel), narrow entry (2nd panel) and highly motile Ki-67+ cells (3rd panel), and composite MAqCI score (4th panel). Black solid line represents the best-fit line while black dotted lines represent the 95% confidence interval. * represents $p<0.05$ and ** represents $p<0.01$. Pearson's correlation was used to assess the significance of the correlation. **(B)** Mean time to recurrence of low versus high percentages of highly

motile cells (1st panel), narrow entry (2nd panel) and highly motile Ki-67+ cells (3rd panel), and composite MAqCI score (4th panel). ** represents $p<0.01$ and *** represents $p<0.001$ as assessed by unpaired student's t-test. **(C)** Percentages of highly motile cells (1st panel), narrow entry (2nd panel) and highly motile Ki-67+ cells (3rd panel), and composite MAqCI score (4th panel) of 5 prospective patient-derived primary GBM cells. Data represent the mean±S.E.M. from $n\geq3$ independent biological replicates. **(D)** Heat maps summarizing the individual MAqCI measurement metrics and composite MAqCI score as described in (3A) for the 5 prospective patients (1st to 4th panels). MAqCI correctly matches the predicted survival (5th panel; red=predicted to be short-term survivors; blue=predicted to be long-term survivors) to the actual survival (6th panel; red=patient deceased before 14.6 months; blue=patient still alive after 14.6 months).

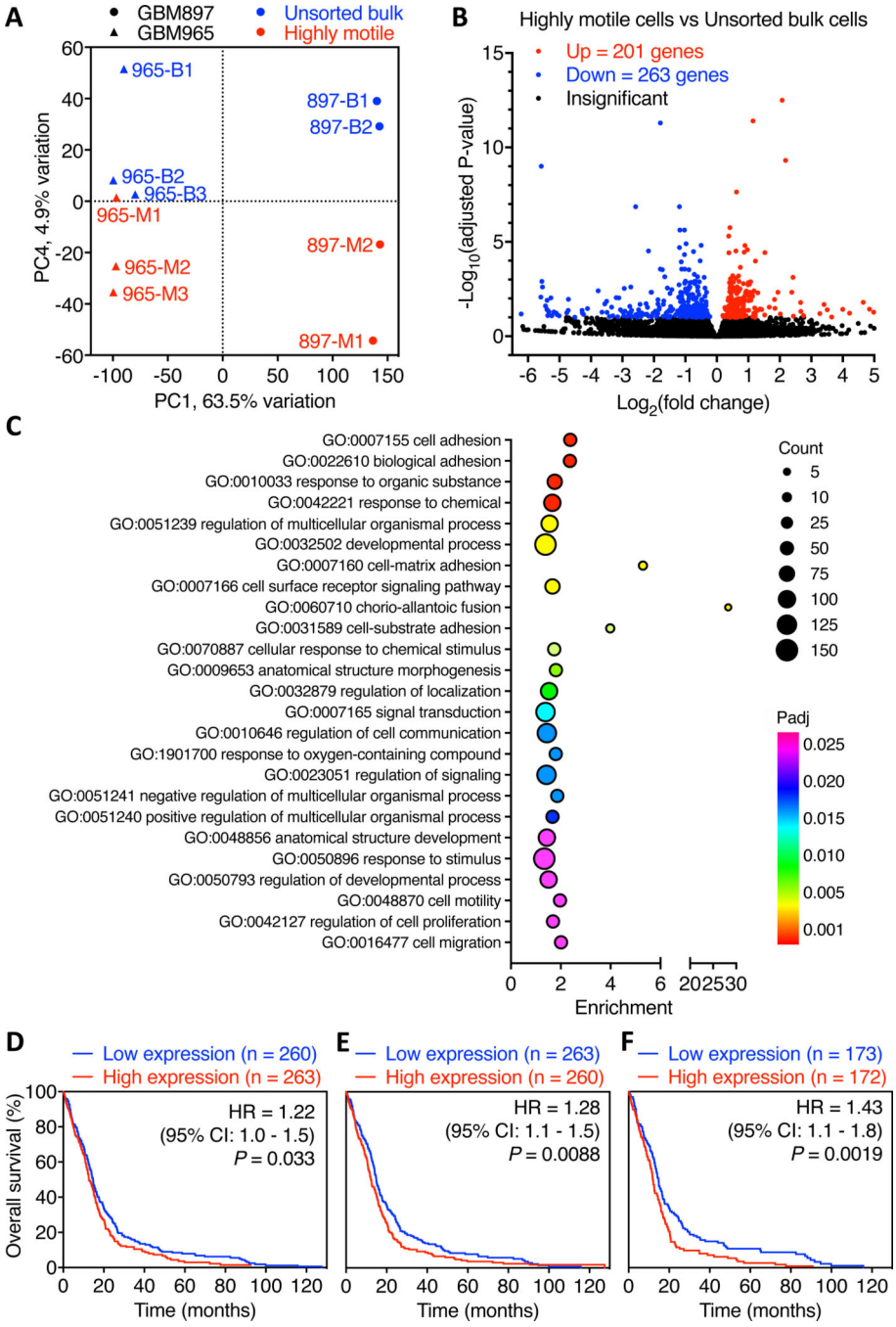

Fig. 5 |. Transcriptome differences between highly motile and unsorted bulk GBM cell subpopulations.

(A) PCA subplot of all highly motile (M) and unsorted bulk (B) cell samples from GBM 965 and 897. Three biological replicate pairs of highly motile and unsorted bulk cell RNA were collected from GBM965 and two biological replicate pairs from GBM897. **(B)** Volcano plot showing DEGs in the highly motile subpopulations, which were identified using FDR<0.1 as a cut-off. **(C)** Scatter plot for top 25 GOBP enrichment terms of DEGs at FDR (Benjamini)<0.05. **(D)** From the 464 DEGs between the highly motile and unsorted bulk cell

subpopulations, expression data for 261 DEGs were available and used to assess the survival time in a cohort of 523 GBM patients. Kaplan-Meier analysis revealed that upregulated DEGs with a $p_{adj}<0.05$ correlated with reduced GBM OS. (**E,F**) Using a collection of 17 upregulated DEGs whose individual expression patterns correlated with OS, a composite score was calculated for each patient. Patients were stratified based on median (**E**) or tercile (**F**) scores. Kaplan-Meier analysis showed significantly worse OS for this collection of 17 upregulated DEGs. Log-rank test was used to calculate P-value and hazard ratio (HR) in (D), (E) and (F).

Table 1 |

Measures of performance for individual MAqCI measurement metrics and composite MAqCI score in classifying the retrospective GBM patient cohort into either short- or long-term survivors.

	Threshold	Sensitivity (%)	Specificity (%)	PPV (%)	NPV (%)	Accuracy (%)	AUC
Highly Motile Cells (%)	3	94.7	55.6	81.8	83.3	82.1	0.69
Narrow Entry (%)	1–3	94.7	44.4	78.3	80.0	78.6	0.74
Highly Motile Ki-67+ (%)	35–45	89.5	66.7	85.0	75.0	82.1	0.77
Unsorted Ki-67+ (%)	45	78.9	66.7	83.3	60.0	75.0	0.69
IDH1 Mutation Status	Yes/No	31.6	55.6	60.0	27.8	37.9	0.44
Cell Index (at 24h)	0.15	5.6	88.9	50.0	32.0	33.3	0.28
Composite MAqCI Score	0.65–0.70	84.2	88.9	94.1	72.7	85.7	0.87

A positive event is defined as short-term survival (<14.6 months) while a negative event is defined as long-term survival (>14.6 months). Sensitivity is defined as the probability of correctly identifying a short-term survival patient from all of the short-term survival patients. Specificity is defined as the probability of correctly identifying a long-term survival patient from all of the long-term survival patients. Positive predictive value (PPV) is defined as the proportion of patients who are predicted to be short-term survival that are truly the short-term survivors. Negative predictive value (NPV) is defined as the proportion of patients who are predicted to be long-term survival that are truly the long-term survivors. Accuracy is defined as the probability of correctly identifying both the short- and long-term survivors from the entire population. Area under curve (AUC) is defined as the area under the receiver operating characteristic curve (ranges from 0 to 1). AUC measures how capable each classifier is able to distinguish and separate the short-term from the long-term GBM survival groups.

Table 2 |

Individual MAqCI measurement metrics, composite MAqCI score and survival outcomes for the prospective GBM patient cohort.

GBM	Highly Motile Cells (%)	Narrow Entry (%)	Highly Motile Ki-67+ (%)	Composite MAqCI Score	Predicted Survival	Actual Survival	Prediction
1295	13.6 ± 2.8	10.8 ± 4.3	71.3 ± 3.3	0.96	Short-Term	Deceased (14.4 Mo)	Correct
1296	9.2 ± 1.6	15.5 ± 6.8	49.4 ± 2.7	0.63	Long-Term	Alive (>14.6 Mo)	Correct
1283	12.2 ± 2.4	0	27.4 ± 6.0	0.08	Long-Term	Deceased (37 Mo)	Correct
1280	3.6 ± 1.6	13.9 ± 9.0	39.6 ± 5.1	0.21	Long-Term	Alive (>14.6 Mo)	Correct
166	9.3 ± 1.6	18.2 ± 3.5	26.9 ± 2.6	0.18	Long-Term	Alive (>14.6 Mo)	Correct